Polytechnic Journal

Polytechnic Journal

Volume 14 | Issue 2 Article 4

Experimental characterization, computational investigation, and structure-property–activity relationship studies of Nickel Ferrite nanostructures

Ali Ben Ahmed

University of Sfax, Faculty of Science of Sfax, Laboratory of Applied Physic, Sfax 3018 Tunisia,

ali.benahmed@isbs.usf.tn

How to Cite This Article

Ahmed, Ali Ben (2024) "Experimental characterization, computational investigation, and structure-property–activity relationship studies of Nickel Ferrite nanostructures," *Polytechnic Journal*: Vol. 14: Iss. 2, Article 4.
DOI: https://doi.org/10.59341/2707-7799.1841

Experimental characterization, computational investigation, and structure-property–activity relationship studies of Nickel Ferrite nanostructures

Data Availability Statement

The data supporting the findings of this study are publicly available and are included within this published article.

AI Usage Declaration

Funding: This study is not funded.

Conflicts of interest: The authors declare that there is no conflict of interest.

Ethical statement: Not applicable

Availability of data and materials: All data generated or analyzed during this study are included in this published article.

Author's contribution statement: The corresponding author done all the work in the Methodology, Investigation, Data curation, Spectroscopies measurement, Validation, formal analysis, Writing and Reviewing, editing, and approval of the final version.

AI Usage Declaration: In this scientific work, generative artificial intelligence (AI) was not used.

Acknowledgments

The author gratefully acknowledges the support of University of Sfax and all individuals who contributed to the successful completion of this study.

ORIGINAL ARTICLE

Experimental Characterization, Computational Investigation, and Structure-property−activity Relationship Studies of Nickel Ferrite Nanostructures

Ali Ben Ahmed

University of Sfax, Faculty of Science of Sfax, Laboratory of Applied Physic, 3018 Sfax, Tunisia

Abstract

Intending to predict the multifunctionality of Nickel ferrite in several technological and medical fields, we have prepared nickel ferrite nanostructure by coprecipitation method. X-ray Diffraction (XRD) is used to determine the crystalline structure and phase composition of materials by analyzing the pattern of X-rays scattered by the atoms within the material. Fourier Transform Infrared Spectroscopy (FTIR) provides information about a material's chemical bonds and functional groups by analyzing how it absorbs infrared light at various wavelengths. Scanning Electron Microscopy (SEM) offers high-resolution images of the material's surface morphology and texture by scanning it with a focused beam of electrons. Transmission Electron Microscopy (TEM) provides detailed images at the atomic or nanometer scale, allowing for the examination of the internal structure, crystallinity, and defects of a material. UV-visible spectroscopy measures the absorbance of ultraviolet or visible light by a material, which can give insight into its electronic structure, band gap, and optical properties. These analyses confirmed the formation of single-phase nickel ferrite nanoparticles in the range 8−14 *nm*. The principal quantum chemical descriptors have been analyzed and discussed. Additionally, the theoretical background of nickel ferrite was carved out using Density Functional Theory (DFT) by evaluating the electronic structure through the Frontier Molecular Orbital, Molecular Electrostatic Potential, Milliken charge distribution, Density of state spectrum, and nonlinear optical parameters embedded within the nickel ferrite molecule. Based on all these results, nickel ferrite can be considered as a multifunctional material.

Keywords: Nanostructures, Nickel ferrite, Computational investigation, Chemical descriptors

1. Introduction

Nanostructured materials exhibit remarkable physical and chemical properties. These properties make them an active field of scientific research due to the variety of their applications in biology, optics, and electronics [1−6]. Nickel ferrite ($NiFe_2O_4$) crystals are one type of nanoparticle that exhibits a variety of different unique phenomena. Among all polymetallic oxides, Nano-sized nickel ferrite has attractive properties. It has been regarded as an excellent candidate in various applications such as catalysis [7−9], sensor technology [10,11], electromagnetic shielding [12−15], water treatment [16−19], biomedical and biotechnology, [20−23]. Outstanding to their minor size and great surface zone, nanomaterials have solid adsorption capacities and reactivity [24−26], and big mobility in solution [27−31]. Nanomaterials effectively remove heavy metals, organic pollutants, inorganic anions, and bacteria [32]. Recently, $NiFe_2O_4$ nanoparticles (NPs), with these remarkable physical and chemical properties of those of free atoms or molecules, have attracted attention for a wide range of potential applications [33−37].

Several synthesis methods can be used for the preparation of $NiFe_2O_4$ NPs, such as coprecipitation [38], citrate precursors [39], mechanical alloys [40], hydrothermal, sol-gel [41], sonochemical [42], reverse micelle [43], and pulsed wire discharge [44]. In the literature, $NiFe_2O_4$ is fully studied experimentally for various applications but has never been

Received 25 August 2024; accepted 30 September 2024.
Available online 22 October 2024
E-mail address: ali.benahmed@isbs.usf.tn.

https://doi.org/10.59341/2707-7799.1841

considered as a nonlinear optical material. Also, in the literature, there are no studies that deal with the chemical reactivity of this molecule. With chemical theory, we can extract more details about the physical properties of materials that can steer the experiment on the road to positive results.

Density Functional Theory (DFT) is a widely used computational modeling method in quantum chemistry and physics, applied to study the electronic structure of many-body systems, primarily atoms, molecules, and condensed matter. It relies on the idea that the properties of a system can be described in terms of its electron density rather than its many-electron wave function, which greatly simplifies calculations [45–48]. DFT, and Time-Dependent Density Functional Theory (TDDFT) which have been used intensively and proved an efficient approach [49–51].

In the present study, we aim to investigate the physical properties of $NiFe_2O_4$. Via the coprecipitation method, the $NiFe_2O_4$ NPs were prepared. The nanoparticle characterization techniques used are X-ray diffraction (XRD), Fourier transform infrared (FTIR) spectroscopy, scanning electron microscope (SEM), Transmission electron microscope (TEM), and UV-visible absorption spectroscopy. The optical properties, the Mulliken charge distribution, the Frontier Molecular Orbitals (FMO), the global reactivities descriptors, the density of state (DOS) spectrum, the energy gap (ΔE), and Molecular Electrostatic Potential (MEP) have been computed by using DFT, and TDDFT methods.

2. Experimental method

2.1. Chemical synthesis

The precursors $NiCl_2.6H_2O$, $FeCl_3.6H_2O$, NaOH, $CH_3(CH_2)_{11}SO_4Na$, glycerol, ethyl acetate, and triethylamine were used for the elaboration of $NiFe_2O_4$ NPs. For 18 h, and at different temperatures of 45°C, 80°C, 100°C, 130°C and 150°C, we heating the mixture. The black precursor was washed carefully.

2.2. Spectroscopic characterizations

The XRD patterns of the synthesis nano-powder were recorded from 10° to 90°. By SEM and TEM, the surface morphology and characteristics of the material were analyzed. To examine functional stretching and bending vibrations of the $NiFe_2O_4$ nano-powder was analyzed by FTIR spectroscopy. The UV-Visible absorption spectrum was recorded in the range $[200 - 1100]$ nm.

3. Computational method

The DFT, and TDDFT/B3LYP/6–311 G(3df) methods implemented in the Gaussian 09 package [52], were used in a computational investigation. The Gauss Sum software tool is used to visualize the density of states (DOS) [53].

4. Results and discussions

4.1. Structure analysis

As can be seen in the XRD patterns of the $NiFe_2O_4$ powders (Fig. 1), all the intensity peaks could be indexed to cubic crystal structure, and Fd-3m space group.

The lattice parameter $a = b = c = 8.438\,\AA$, a volume of cell $600.784\,\AA^3$, and the ideal orientation of the nanopowders is in the direction (311) as also shown. The average crystallite size of NPs, is $D = 8.517\,nm$. No impurity was observed in XRD patterns, indicating the purity of prepared $NiFe_2O_4$. The most stable optimized geometry of the $NiFe_2O_4$ cluster is given in Fig. 2.

4.2. Vibrational spectroscopic analysis

The FTIR spectrum is shown in Fig. 3, and the tentative assignment was inserted in Table 1. A characteristic peak for the $NiFe_2O_4$ NPs, is shows below 700 cm^{-1} [54]. At 838 cm^{-1} and 676 cm^{-1}, a characteristic peak is contributed by the bending and stretching modes of Ni–O and Fe–O–Fe. Both simulated spectrum (see Fig. 4) clearly shows the various stretching, deformation, and bending frequencies of functional material nickel ferrite. The

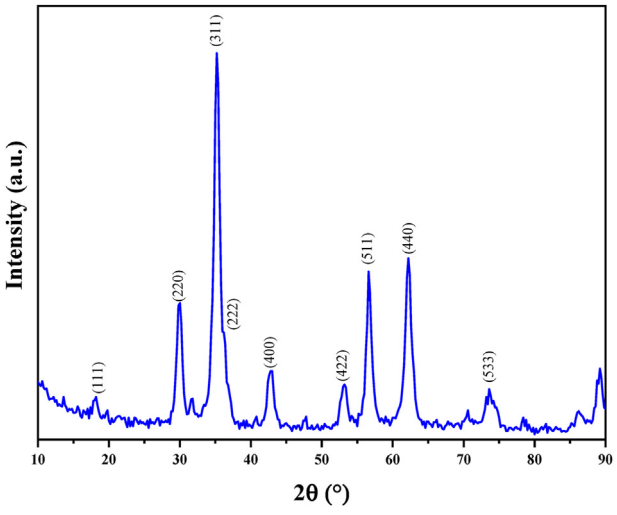

Fig. 1. XRD pattern of $NiFe_2O_4$ NPs.

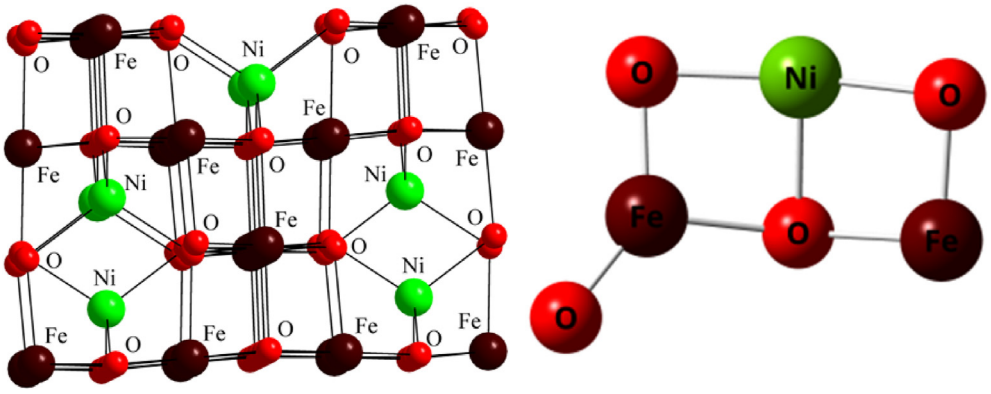

Fig. 2. Optimized geometry in the ground state of $NiFe_2O_4$.

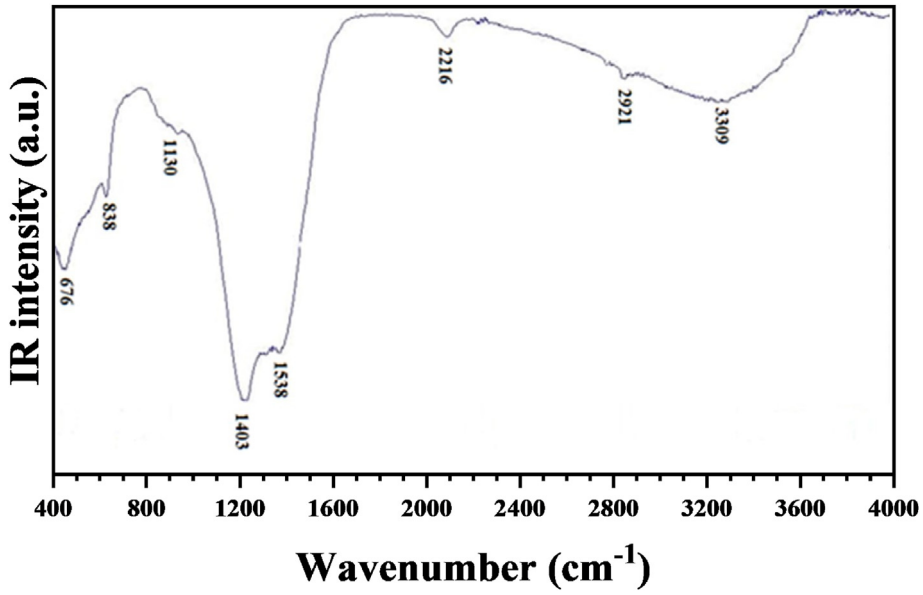

Fig. 3. Experimental FTIR spectrum of $NiFe_2O_4$ NPs.

vibrational frequencies are start from 70 cm^{-1} to 1105 cm^{-1}. The four bands appeared at 1105 cm^{-1}, 836 cm^{-1}, 789 cm^{-1}, and 717 cm^{-1} are considered to be highly characteristic frequencies for nickel ferrite. In Fig. 4, the medium band appeared in the frequency range $596 - 511\ cm^{-1}$ are assigned to nickel oxygen and iron oxygen stretching, while the low band appeared in the frequency range $77 - 377\ cm^{-1}$ are assigned to the metal oxygen vibration. All peak appeared in Figs. (3,4) are assigned in Table 1.

4.3. Scanning Electron Microscopy analysis

The SEM image and the corresponding particle size histogram of the $NiFe_2O_4$ nano-powder are presented in Fig. 5. The SEM image of prepared NPs shows the sphere-shaped NPs agglomerated together to give better surface area. The NPs size was found to be 48.76 *nm*.

4.4. Transmission Electron Microscopy analysis

The TEM image of the $NiFe_2O_4$ nano-powder and the corresponding particle size histogram are shown in Fig. 6. The average particle size identified by the TEM image was found to be 14 *nm*.

4.5. Milliken charge distribution

The Mulliken atomic charge distribution, shown in Fig. 7, is related to the chemical bonds present in the optimized compound. This distribution quantifies how the electronic structure charges under atomic displacement. It affects dipole moment, polarizability, electronic structure, and more properties of

Table 1. Observed and calculated frequencies (cm^{-1}) of $NiFe_2O_4$.

Experimental	DFT		Assignments
	IR	Raman	
3309	–	–	N–H stretching
2921	–	–	C–H stretching
2216	–	–	C=C stretching
1538	–	–	N–O stretching
1403	–	–	C–H bending
1130	–	–	C–N stretching
–	1105	1105	Fe–O stretching
838	836	836	Ni–O in plan bending
–	789	789	(O–Ni–O) deformation
676	717	717	(Fe–O–Fe) asymmetric stretching
–	596	596	(O–Fe–O) deformation
–	538	538	(O–Ni–O) symmetric stretching
–	511	511	(O–Ni–O) asymmetric stretching
–	–	377	(Fe–O–Fe) twisting
–	–	278	(Fe–O–Fe) scissoring
–	–	250	(Fe–O–Fe) symmetric stretching
–	–	222	(Ni–O–Fe) deformation
–	–	208	Fe–O in plan bending
–	–	99	(Fe–O–Fe) deformation
–	–	77	Fe–O out of plan bending

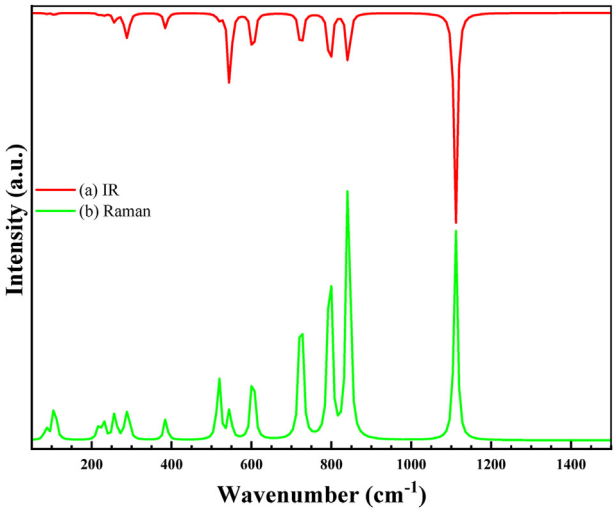

Fig. 4. Simulated IR (a) and Raman (b) spectra of $NiFe_2O_4$.

molecular systems [55]. The total charge of the $NiFe_2O_4$ cluster is zero, meaning it is neutral as a whole. The oxygen atoms are electronegative, meaning they tend to attract electrons. As a result, the electron density is delocalized over the oxygen atoms. Both iron (Fe) and nickel (Ni) atoms exhibit positive charges, indicating a loss of electron density. However, the atoms that are directly attached to oxygen atoms tend to have even more positive charges, due to the strong electron-withdrawing effect of the oxygen atoms [56,57]. The variation in charge distribution within the cluster reflects the differences in how the metal atoms interact with the surrounding oxygen atoms.

4.6. Molecular electrostatic potential

The MEP (Fig. 8) analysis provides information on the electrophilic and nucleophilic reactivities. Fig. 8 illustrates the reactive sites of the iron, nickel, and oxygen atoms in the $NiFe_2O_4$ cluster, highlighting the regions susceptible to various chemical attacks. The electrophilic region is predominantly concentrated on the oxygen atom, whereas the nucleophilic region is associated with the iron and nickel atoms that are bonded to oxygen. The presence of a positive region extending over the iron and nickel atoms suggests a potential site for electrophilic attack.

4.7. Linear and nonlinear optical properties

4.7.1. UV-visible spectra

The UV-visible spectroscopy results for $NiFe_2O_4$ NPs in Fig. 9(a and b) indicate both experimental and computed outcomes, showing how the material interacts with light. The absence of absorption bands in the visible region suggests that $NiFe_2O_4$ is transparent to visible light, making it ideal for photonic and optical applications. This implies that the NPs have a high potential for use in devices where minimal light absorption is essential, such as in optical filters or transparent coatings. Moreover, the interaction of $NiFe_2O_4$ NPs with light at a specific wavelength might correspond to absorption in the UV range, which could suggest possible applications in UV filtering or sensing technologies. The material's behavior can also be leveraged for advanced optical devices where controlled interaction with light is critical [58–60].

The optical absorption spectrum of $NiFe_2O_4$ film measured at room temperature (see Fig. 9(a)) displays several distinct bands, indicating the presence of multiple electronic transitions. The first observed absorption band $\lambda_1 = 543\ nm\ (2.28\ eV)$ corresponds to an electronic transition from the HOMO (highest occupied molecular orbital) to the LUMO (lowest unoccupied molecular orbital). The second observed absorption band $\lambda_2 = 426\ nm\ (2.91\ eV)$ is associated with a charge transfer from the $4s^2$ atomic state in Fe to $2p^4$ atomic state in O. The third observed absorption band $\lambda_3 = 320\ nm\ (3.87\ eV)$ is related to a charge transfer from the $4s^2$ atomic state in Ni to $2p^4$ atomic state in O. The fourth observed absorption band $\lambda_4 = 252\ nm\ (4.92\ eV)$ is attributed to a

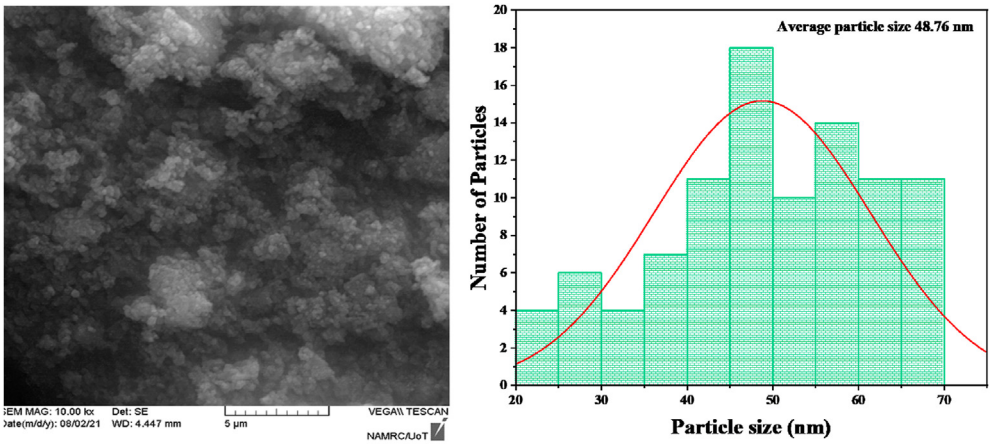

Fig. 5. SEM image and corresponding particle size histogram of $NiFe_2O_4$ NPs.

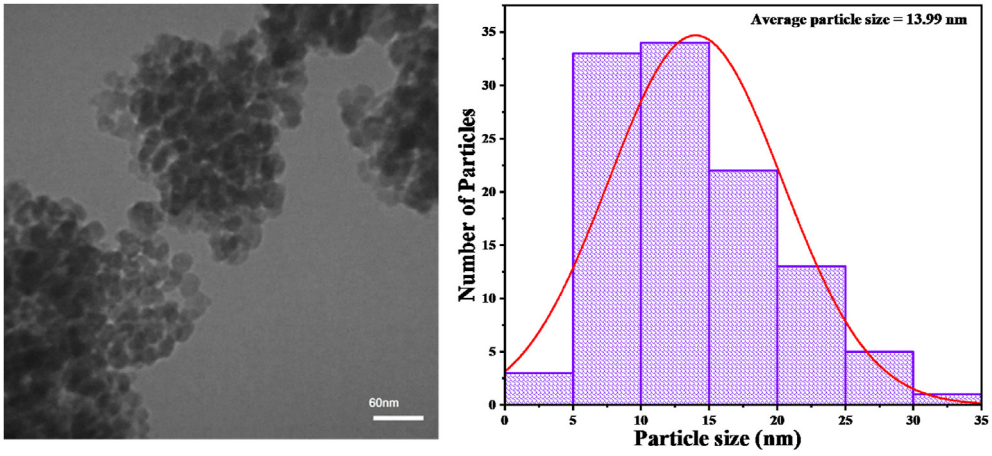

Fig. 6. TEM image and corresponding particle size histogram of $NiFe_2O_4$ NPs.

conjugate charge transfer involving all three constituent atoms (Ni, Fe, and O).

According to the computational result (see Fig. 9(b)), the simulated spectrum predicts two intense transitions. The first absorption band centered at 322 nm (3.85 eV) matches the observed $\lambda_3 = 320\ nm$. The second observed absorption band centered at 402 nm (3.08 eV) matches $\lambda_2 = 426\ nm$. Additionally, the band at 2.56 eV (computed) aligns with the experimentally observed $\lambda_1 = 543\ nm$, confirming it as an electronic transition from the

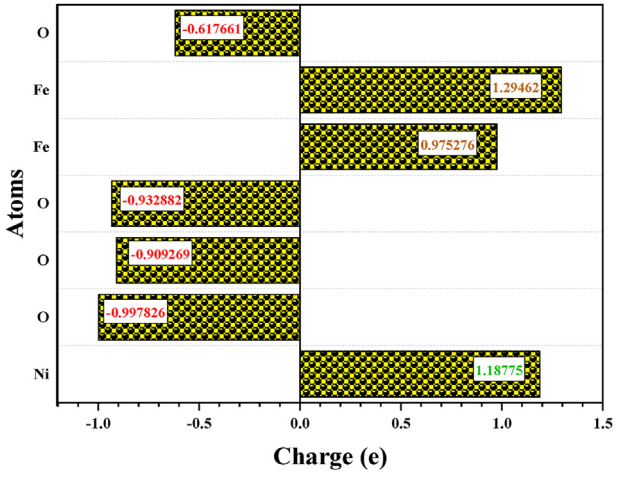

Fig. 7. Atomic charge distribution in computed geometry of $NiFe_2O_4$.

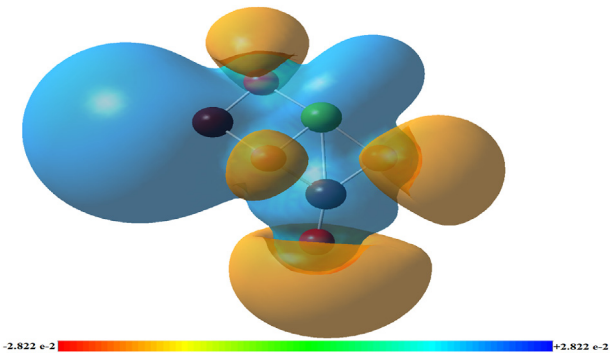

Fig. 8. MEP plot of $NiFe_2O_4$.

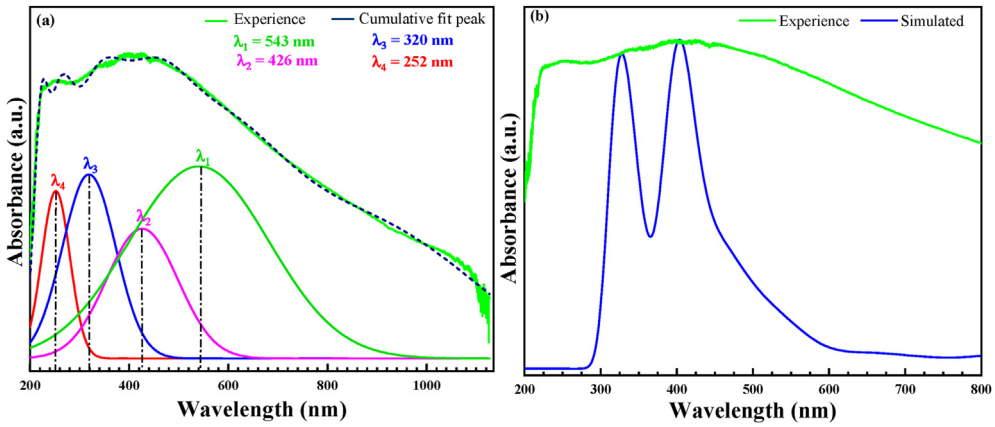

Fig. 9. The experimental (a) and simulated (b) UV-Visible absorption spectra of $NiFe_2O_4$.

HOMO to the LUMO. The Fe−O bond angle plays a significant role in shaping the electronic structure of the $NiFe_2O_4$ cluster. Although DFT-calculated bond lengths differ from experimental values, their effect is neglected in this analysis. In summary, the experimental optical absorption bands are well-aligned with the simulated spectrum, and the electronic transitions are primarily due to charge transfer processes involving the Ni, Fe, and O atoms.

4.7.2. DOS spectrum and optical band gap analysis

This section provides insight into both the experimental and theoretical analysis of the bandgap energy of $NiFe_2O_4$, which is crucial for understanding its optical and electrical properties. The optical bandgap is measured experimentally to be $E_g = 2.45\ eV$ using the Tauc formula, which is consistent with the values for bulk $NiFe_2O_4$. This agreement indicates the reliability of the experimental technique. According to the DOS spectrum, a computational approach estimates the bandgap as $2.56\ eV$, which is very close to the experimental value. The small difference between experimental and computational bandgaps is attributed to the fact that the computational simulation is performed in the gas phase, without considering the neighboring atom effects that are present in the actual material. The HOMO (Highest Occupied Molecular Orbital) is slightly delocalized in oxygen atoms but shows a greater influence on the iron (Fe) atoms. The LUMO (Lowest Unoccupied Molecular Orbital) is primarily delocalized on the nickel (Ni) atoms (see Fig. 10).

The comparison between experimental and theoretical data shows close agreement, and the discussion of HOMO/LUMO highlights the roles of different atoms in influencing the electronic structure and stability of $NiFe_2O_4$. This understanding is fundamental to optimizing the material's properties for specific applications [61–64].

4.7.3. The global reactivity descriptors

The global reactivity descriptors were calculated for the study compound. All quantum chemical parameters are listed in Table 2. The information provided suggests that $NiFe_2O_4$ NPs exhibit several key properties that could make them effective for antibacterial applications. The ionization potential $(I_P = 5.89\ eV)$ and electronegativity $(\chi = 4.61)$ have high values indicate a strong tendency of the $NiFe_2O_4$ molecule to attract and hold onto electrons. This is important in the context of antibacterial activity because such properties can influence how the NPs interact with bacterial cell membranes or reactive species in the environment. The electrophilicity index $(\omega = 4.15)$ measures the ability of the molecule to accept electrons, and a high value means the molecule can act as an electrophile, making it reactive toward nucleophilic biological targets. This could contribute to its antibacterial properties. The moderate band gap energy $(\Delta E_{H-L} = 2.56\ eV)$ suggests that $NiFe_2O_4$ has a balance between being a good insulator and a semiconductor, which could enhance its interaction with biological systems and possibly generate reactive oxygen species (ROS), contributing to antibacterial effects. The chemical hardness $(\eta = 2.56\ eV)$ and the softness $(\sigma = 0.39\ eV)$ reflect the molecule's resistance to deformation or polarization. Higher hardness indicates that the molecule is stable, while lower softness reflects the limited ease with which the electron density can be redistributed. Together, these properties suggest that $NiFe_2O_4$ has a stable structure but also retains the ability to facilitate charge transfer, which could promote biological activity. The low softness $(\sigma = 0.39\ eV)$ and negative

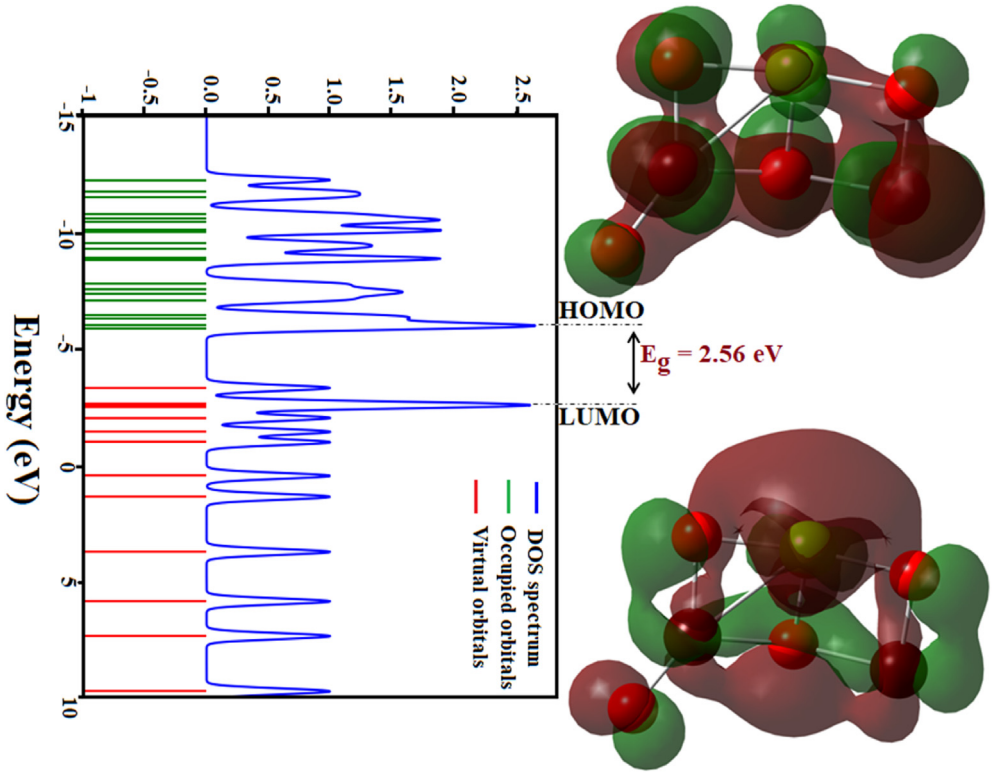

Fig. 10. The FMO and DOS spectrum of $NiFe_2O_4$.

chemical potential $\mu\ (-4.61\ eV)$ indicate that $NiFe_2O_4$ is stable and has a low risk of being highly toxic [65,66]. The combination of high stability, efficient charge transfer, moderate toxicity, and dual reactivity suggests that $NiFe_2O_4$ NPs could be highly effective in antibacterial applications [67].

4.7.4. Nonlinear optical parameters

The material $NiFe_2O_4$ shows promising potential in the field of optoelectronics due to its high degree of hyperpolarizability, which is crucial for nonlinear optical (NLO) applications [68–71]. According to the calculated optical parameters (see Table 3), the total dipole moment is $\mu_{tot} = 4.2172\ D$, with the maximum contribution of 3.9539 D along the μ_x direction, while the values in other directions are moderate. The total polarizability is $\alpha_{tot} = 9.095 \times 10^{-24}\ esu$, with the diagonal components playing a significant role. The average second hyperpolarizability is $\langle\gamma\rangle$ 0.2366 ×

Table 2. Global reactivities parameters of $NiFe_2O_4$.

Parameters	Values
$E_{HOMO}\ (eV)$	−5.89
$E_{LUMO}\ (eV)$	−3.33
$\Delta E\ (eV)$	2.56
$I_P = -E_{HOMO}$	5.89
$E_A = -E_{LUMO}$	3.33
$\chi = -\frac{E_{LUMO}+E_{HOMO}}{2}$	4.61
$\mu = \frac{E_{LUMO}+E_{HOMO}}{2}$	−4.61
$\eta = \frac{E_{LUMO}-E_{HOMO}}{2}$	2.56
$\sigma = \frac{1}{\eta}$	0.39
$\omega = \frac{\mu^2}{2\eta}$	4.15

Table 3. Dipole moment, static polarizability, and second hyperpolarizability components of Nickel Ferrite.

Properties	Parameters	Values
$\mu_{tot}\ (D)$	μ_x	3.9539
	μ_y	−1.4321
	μ_z	0.3161
	μ_{tot}	4.2172
$\alpha_{tot}\ (\times 10^{-24}\ esu)$	α_{xx}	10.029
	α_{yy}	8.341
	α_{zz}	8.915
	α_{xy}	1.151
	α_{yz}	0.010
	α_{xz}	0.005
	α_{tot}	9.095
$\langle\gamma\rangle\ (\times 10^{-36}\ esu)$	γ_{xxxx}	0.500
	γ_{yyyy}	0.172
	γ_{zzzz}	0.037
	γ_{xxyy}	0.116
	γ_{xxzz}	0.085
	γ_{yyzz}	0.036
	$\langle\gamma\rangle$	0.2366

10^{-36} *esu*, indicating a substantial nonlinear optical response. These results suggest that $NiFe_2O_4$ possesses strong nonlinear optical properties, making it a viable candidate for optoelectronic and photonic applications, especially in devices requiring both linear and nonlinear optical properties. By doping with electron-rich elements, its potential could be further enhanced for use in advanced NLO materials [72].

5. Conclusions

The $NiFe_2O_4$ NPs synthesized through the coprecipitation method demonstrate promising optical properties for optoelectronic and photonic applications, as confirmed through both experimental and theoretical investigations. The wide bandgap of 2.45 eV (with a computed value of 2.56 eV) indicates good stability under visible light, enhancing the material's potential for real-world applications. The study further explores the spectroscopic properties and global reactivity descriptors, revealing that $NiFe_2O_4$ exhibits dual characteristics, making it highly versatile for various applications. The theoretical analysis suggests that bandgap, polarizability, and hardness are key chemical descriptors that can also help identify compounds with potential biological activity. Thus, $NiFe_2O_4$ NPs hold significant promise in both technological and biological fields.

Ethical statement

Not applicable.

Funding

This study is not funded.

Availability of data and materials

All data generated or analyzed during this study are included in this published article.

Author's contribution statement

The corresponding author done all the work in the Methodology, Investigation, Data curation, Spectroscopies measurement, Validation, formal analysis, Writing and Reviewing, editing, and approval of the final version.

AI usage declaration

In this scientific work, generative artificial intelligence (AI) was not used.

Conflicts of interest

The authors declare that there is no conflict of interest.

References

[1] Karakaş ZK, Boncukçuoğlu R, Karakaş İH. The effects of fuel type in synthesis of NiFe 2 O 4 nanoparticles by microwave assisted combustion method. J Phys Conf 2016;707:012046. https://doi.org/10.1088/1742-6596/707/1/012046.

[2] Pourshojaei Y, Zolala F, Eskandari K, Talebi M, Morsali L, Amiri M, Khodadadi A, Shamsimeymandi R, Faghih-Mirzaei E, Asadipour A. Nickel Ferrite (NiFe 2 O 4) Nanoparticles as Magnetically Recyclable Nanocatalyst for Highly Efficient Synthesis of 4H-Chromene Derivatives. J Nanosci Nanotechnol 2020;20:3206–16. https://doi.org/10.1166/jnn.2020.17396.

[3] Sen R, Jain P, Patidar R, Srivastava S, Rana RS, Gupta N. Synthesis and Characterization of Nickel Ferrite (NiFe2O4) Nanoparticles Prepared by Sol- Gel Method. Mater Today Proc 2015;2:3750–7. https://doi.org/10.1016/j.matpr.2015.07.165.

[4] George M, Mary John A, Nair SS, Joy PA, Anantharaman MR. Finite size effects on the structural and magnetic properties of sol–gel synthesized NiFe2O4 powders. J Magn Magn Mater 2006;302:190–5. https://doi.org/10.1016/j.jmmm.2005.08.029.

[5] Dongale TD, Khot SS, Patil AA, Wagh SV, Patil PB, Dubal DP, Kim TG. Bifunctional nanoparticulated nickel ferrite thin films: Resistive memory and aqueous battery applications. Mater Des 2021;201:109493. https://doi.org/10.1016/j.matdes.2021.109493.

[6] Kurda AH, Kakil SA, Hassan YM. High Responsivity of Sol-gel TiO2NPs/Si Photodetectors Deposited by Spin Coating Method. Polytechnic Journal 2024;14. https://doi.org/10.59341/2707-7799.1832.

[7] Ramankutty C, Sugunan S. Surface properties and catalytic activity of ferrospinels of nickel, cobalt and copper, prepared by soft chemical methods. Appl Catal Gen 2001;218:39–51. https://doi.org/10.1016/S0926-860X(01)00610-X.

[8] Hong D, Yamada Y, Nagatomi T, Takai Y, Fukuzumi S. Catalysis of Nickel Ferrite for Photocatalytic Water Oxidation Using [Ru(bpy) 3] 2+ and S 2 O 8 2. J Am Chem Soc 2012;134:19572–5. https://doi.org/10.1021/ja309771h.

[9] Xiao Y, Zai J, Tian B, Qian X. Formation of NiFe2O4/Expanded Graphite Nanocomposites with Superior Lithium Storage Properties. Nano-Micro Lett 2017;9:34. https://doi.org/10.1007/s40820-017-0127-7.

[10] Zhang L, Jiao W. The effect of microstructure on the gas properties of NiFe2O4 sensors: Nanotube and nanoparticle. Sensor Actuator B Chem 2015;216:293–7. https://doi.org/10.1016/j.snb.2015.04.049.

[11] Joshi S, Kamble VB, Kumar M, Umarji AM, Srivastava G. Nickel substitution induced effects on gas sensing properties of cobalt ferrite nanoparticles. J Alloys Compd 2016;654:460–6. https://doi.org/10.1016/j.jallcom.2015.09.119.

[12] He J-Z, Wang X-X, Zhang Y-L, Cao M-S. Small magnetic nanoparticles decorating reduced graphene oxides to tune the electromagnetic attenuation capacity. J Mater Chem C 2016;4:7130–40. https://doi.org/10.1039/C6TC02020H.

[13] Biswas S, Kar GP, Bose S. Microwave absorbers designed from PVDF/SAN blends containing multiwall carbon nanotubes anchored cobalt ferrite via a pyrene derivative. J Mater Chem A 2015;3:12413–26. https://doi.org/10.1039/C5TA02177D.

[14] Madhu BJ, Ashwini ST, Shruthi B, Divyashree BS, Manjunath A, Jayanna HS. Structural, dielectric and electromagnetic shielding properties of Ni–Cu nanoferrite/PVP composites. Mater Sci Eng, B 2014;186:1–6. https://doi.org/10.1016/j.mseb.2014.02.018.

[15] Sun J, Ma F. Improved shielding and filtering applied to immunity enhancement of underground gas sensors. J China Univ Mining Technol 2008;18:220–3. https://doi.org/10.1016/S1006-1266(08)60046-2.

[16] Wang Z, Du Y, Liu Y, Zou B, Xiao J, Ma J. Degradation of organic pollutants by NiFe 2 O 4 /peroxymonosulfate: efficiency, influential factors and catalytic mechanism. RSC Adv 2016;6:11040–8. https://doi.org/10.1039/C5RA21117D.

[17] Zhao H, Dong Y, Wang G, Jiang P, Zhang J, Wu L, Li K. Novel magnetically separable nanomaterials for heterogeneous catalytic ozonation of phenol pollutant: NiFe2O4 and their performances. Chem Eng J 2013;219:295–302. https://doi.org/10.1016/j.cej.2013.01.019.
[18] Xu S, Shangguan W, Yuan J, Chen M, Shi J, Jiang Z. Synthesis and performance of novel magnetically separable nanospheres of titanium dioxide photocatalyst with egg-like structure. Nanotechnology 2008;19:095606. https://doi.org/10.1088/0957-4484/19/9/095606.
[19] Xu S, Shangguan W, Yuan J, Chen M, Shi J. Preparations and photocatalytic properties of magnetically separable nitrogen-doped TiO2 supported on nickel ferrite. Appl Catal B Environ 2007;71:177–84. https://doi.org/10.1016/j.apcatb.2006.09.004.
[20] Singh J, Roychoudhury A, Srivastava M, Chaudhary V, Prasanna R, Lee DW, Lee SH, Malhotra BD. Highly Efficient Bienzyme Functionalized Biocompatible Nanostructured Nickel Ferrite–Chitosan Nanocomposite Platform for Biomedical Application. J Phys Chem C 2013;117:8491–502. https://doi.org/10.1021/jp312698g.
[21] Kalia S, Kango S, Kumar A, Haldorai Y, Kumari B, Kumar R. Magnetic polymer nanocomposites for environmental and biomedical applications. Colloid Polym Sci 2014;292:2025–52. https://doi.org/10.1007/s00396-014-3357-y.
[22] Sanpo N, Berndt CC, Wen C, Wang J. Transition metal-substituted cobalt ferrite nanoparticles for biomedical applications. Acta Biomater 2013;9:5830–7. https://doi.org/10.1016/j.actbio.2012.10.037.
[23] Ahamed M, Akhtar MJ, Alhadlaq HA, Khan MAM, Alrokayan SA. Comparative cytotoxic response of nickel ferrite nanoparticles in human liver HepG2 and breast MFC-7 cancer cells. Chemosphere 2015;135:278–88. https://doi.org/10.1016/j.chemosphere.2015.03.079.
[24] Doust Mohammadi M, Abdullah HY. Non-covalent interactions of cysteine onto C60, C59Si, and C59Ge: a DFT study. J Mol Model 2021;27:330. https://doi.org/10.1007/s00894-021-04960-5.
[25] Doust Mohammadi M, Abdullah HY. The adsorption of bromochlorodifluoromethane on pristine and Ge-doped silicon carbide nanotube: a PBC-DFT, NBO, and QTAIM study. Struct Chem 2021;32:481–94. https://doi.org/10.1007/s11224-020-01646-1.
[26] Doust Mohammadi M, Abdullah HY. The Adsorption of Chlorofluoromethane on Pristine, Al-, Ga-, P-, and As-doped Boron Nitride Nanotubes: A PBC-DFT, NBO, and QTAIM Study. ChemistrySelect 2020;5:12115–24. https://doi.org/10.1002/slct.202003367.
[27] Kinemuchi Y, Ishizaka K, Suematsu H, Jiang W, Yatsui K. Magnetic properties of nanosize NiFe2O4 particles synthesized by pulsed wire discharge. Thin Solid Films 2002;407:109–13. https://doi.org/10.1016/S0040-6090(02)00021-4.
[28] Brook RJ, Kingery WD. Nickel Ferrite Thin Films: Microstructures and Magnetic Properties. J Appl Phys 1967;38:3589–94. https://doi.org/10.1063/1.1710177.
[29] Jacob J, Khadar MA. Investigation of mixed spinel structure of nanostructured nickel ferrite. J Appl Phys 2010;107. https://doi.org/10.1063/1.3429202.
[30] de Paiva JAC, Graça MPF, Monteiro J, Macedo MA, Valente MA. Spectroscopy studies of NiFe2O4 nanosized powders obtained using coconut water. J Alloys Compd 2009;485:637–41. https://doi.org/10.1016/j.jallcom.2009.06.052.
[31] Zekić E, Vuković Ž, Halkijević I. Application of nanotechnology in wastewater treatment. Journal of the Croatian Association of Civil Engineers 2018;70:315–23. https://doi.org/10.14256/JCE.2165.2017.
[32] Abdelbasir SM, Shalan AE. An overview of nanomaterials for industrial wastewater treatment. Kor J Chem Eng 2019;36:1209–25. https://doi.org/10.1007/s11814-019-0306-y.
[33] Masood MH, Haleem N, Shakeel I, Jamal Y. Carbon dioxide conversion into the reaction intermediate sodium formate for the synthesis of formic acid. Res Chem Intermed 2020;46:5165–80. https://doi.org/10.1007/s11164-020-04255-z.
[34] Hu J, Lo I, Chen G. Comparative study of various magnetic nanoparticles for Cr(VI) removal. Separ Purif Technol 2007;56:249–56. https://doi.org/10.1016/j.seppur.2007.02.009.
[35] Moradmard H, Shayesteh SF. The Variation of Magnetic Properties of Nickel Ferrite by Annealing. Manufac Sci Technol 2015;3:141–5. https://doi.org/10.13189/mst.2015.030411.
[36] Phul R, Khan MAM, Sardar M, Ahmed J, Ahmad T. Multifunctional Electrochemical Properties of Synthesized Non-Precious Iron Oxide Nanostructures. Crystals 2020;10:751. https://doi.org/10.3390/cryst10090751.
[37] Giraldo L, Erto A, Moreno-Piraján JC. Magnetite nanoparticles for removal of heavy metals from aqueous solutions: synthesis and characterization. Adsorption 2013;19:465–74. https://doi.org/10.1007/s10450-012-9468-1.
[38] Sagadevan S, Chowdhury ZZ, Rafique RF. Preparation and Characterization of Nickel ferrite Nanoparticles via Co-precipitation Method. Mater Res 2018;21. https://doi.org/10.1590/1980-5373-mr-2016-0533.
[39] Prasad S, Gajbhiye N. Magnetic studies of nanosized nickel ferrite particles synthesized by the citrate precursor technique. J Alloys Compd 1998;265:87–92. https://doi.org/10.1016/S0925-8388(97)00431-3.
[40] Hajalilou A, Hashim M, Ebrahimi-Kahrizsangi R, Mohamed Kamari H, Kanagesan S. Parametric optimization of NiFe2O4 nanoparticles synthesized by mechanical alloying. Materials Science-Poland 2014;32:281–91. https://doi.org/10.2478/s13536-013-0173-x.
[41] Majid F, Rauf J, Ata S, Bibi I, Malik A, Ibrahim SM, Ali A, Iqbal M. Synthesis and characterization of NiFe2O4 ferrite: Sol–gel and hydrothermal synthesis routes effect on magnetic, structural and dielectric characteristics. Mater Chem Phys 2021;258:123888. https://doi.org/10.1016/j.matchemphys.2020.123888.
[42] Amulya MAS, Nagaswarupa HP, Kumar MRA, Ravikumar CR, Prashantha SC, Kusuma KB. Sonochemical synthesis of NiFe2O4 nanoparticles: Characterization and their photocatalytic and electrochemical applications. Applied Surface Science Advances 2020;1:100023. https://doi.org/10.1016/j.apsadv.2020.100023.
[43] Kale A, Gubbala S, Misra RDK. Magnetic behavior of nanocrystalline nickel ferrite synthesized by the reverse micelle technique. J Magn Magn Mater 2004;277:350–8. https://doi.org/10.1016/j.jmmm.2003.11.015.
[44] Lee PY, Ishizaka K, Suematsu H, Jiang W, Yatsui K. Magnetic and Gas Sensing Property of Nanosized NiFe2O4 Powders Synthesized by Pulsed Wire Discharge. J Nanoparticle Res 2006;8:29–35. https://doi.org/10.1007/s11051-005-5427-z.
[45] Mohammadi MD, Abdullah HY, Biskos G, Bhowmick S. Enhancing the absorption of 1-chloro-1,2,2,2-tetrafluoroethane on carbon nanotubes: an ab initio study. Bull Mater Sci 2021;44:198. https://doi.org/10.1007/s12034-021-02472-9.
[46] Doust Mohammadi M, Abdullah HY. Adsorption of 1-chloro-1,2,2,2-tetrafluoroethane on pristine, Al, Ga-doped boron nitride nanotubes: a study involving PBC-DFT, NBO analysis, and QTAIM. Can J Chem 2021;99:51–62. https://doi.org/10.1139/cjc-2020-0309.
[47] Mohammadi MD, Salih IH, Abdullah HY. An Ultimate Investigation on the Adsorption of Amantadine on Pristine and Decorated Fullerenes C59X (X=Si, Ge, B, Al, Ga, N, P, and As): A DFT, NBO, and QTAIM Study. J Comput Biophy Chem 2021;20:23–39. https://doi.org/10.1142/S2737416521500022.
[48] Doust Mohammadi M, Abdullah HY, Kalamse V, Chaudhari A. Interaction of Fluorouracil drug with boron nitride nanotube, Al doped boron nitride nanotube and BC2N nanotube. Comput Theoretic Chem 2022;1212:113699. https://doi.org/10.1016/j.comptc.2022.113699.
[49] Mohammadi MD, Salih IH, Abdullah HY. The adsorption of chlorofluoromethane on pristine and Ge-doped silicon carbide nanotube: a PBC-DFT, NBO, and QTAIM study. Mol Simulat 2020;46:1405–16. https://doi.org/10.1080/08927022.2020.1834103.

[50] Mohammadi MD, Abdullah HY. DFT Study for Adsorbing of Bromine Monochloride onto BNNT (5,5), BNNT (7,0), BC 2 NNT (5,5), and BC 2 NNT (7,0). J Comput Biophy Chem 2021; 20:765–83. https://doi.org/10.1142/S2737416521500472.
[51] Doust Mohammadi M, Abdullah HY. Intermolecular Interactions between Serine and C60, C59Si, and C59Ge: a DFT Study. Silicon 2022;14:6075–88. https://doi.org/10.1007/s12633-021-01408-6.
[52] Frisch MJ, et al. Gaussian 09, revision A.02, vol. 1. Wallingford: Gaussian, F Inc; 2009. p. 1–44.
[53] O'boyle NM, Tenderholt AL, Langner KM. cclib: A library for package-independent computational chemistry algorithms. J Comput Chem 2008;29:839–45. https://doi.org/10.1002/jcc.20823.
[54] Sridharan K, Agarwal M, Philip J, Endo T, Philip R. Optical Nonlinearity in NiFe2O4 Nanoparticles. Trans Mater Res Soci Japan 2010;35:159–62. https://doi.org/10.14723/tmrsj.35.159.
[55] Govindarajan M, Karabacak M. Spectroscopic properties, NLO, HOMO–LUMO and NBO analysis of 2,5-Lutidine. Spectrochim Acta Mol Biomol Spectrosc 2012;96:421–35. https://doi.org/10.1016/j.saa.2012.05.067.
[56] Ramalingam S, Karabacak M, Periandy S, Puviarasan N, Tanuja D. Spectroscopic (infrared, Raman, UV and NMR) analysis, Gaussian hybrid computational investigation (MEP maps/HOMO and LUMO) on cyclohexanone oxime. Spectrochim Acta Mol Biomol Spectrosc 2012;96:207–20. https://doi.org/10.1016/j.saa.2012.03.090.
[57] Ramalingam S, Periandy S, Govindarajan M, Mohan S. FTIR and FTRaman spectra, assignments, ab initio HF and DFT analysis of 4-nitrotoluene. Spectrochim Acta Mol Biomol Spectrosc 2010;75:1308–14. https://doi.org/10.1016/j.saa.2009.12.072.
[58] Alkalah C. The oxford handbook of nanoscience and technology: materials: structures, properties and characterization techniques. 2016.
[59] Agarwal S, Jangir LK, Rathore KS, Kumar M, Awasthi K. Morphology-dependent structural and optical properties of ZnO nanostructures. Appl Phys A 2019;125:553. https://doi.org/10.1007/s00339-019-2852-x.
[60] Monat JE, Rodriguez JH, McCusker JK. Ground- and Excited-State Electronic Structures of the Solar Cell Sensitizer Bis(4,4′-dicarboxylato-2,2′-bipyridine)bis(isothiocyanato)ruthenium(II). J Phys Chem 2002;106:7399–406. https://doi.org/10.1021/jp020927g.
[61] Reddy RR, Nazeer Ahammed Y. A study on the Moss relation. Infrared Phys Technol 1995;36:825–30. https://doi.org/10.1016/1350-4495(95)00008-M.
[62] Tian L, Lin B, Wu L, Li K, Liu H, Yan J, Liu X, Xi Z. Neurotoxicity induced by zinc oxide nanoparticles: age-related differences and interaction. Sci Rep 2015;5:16117. https://doi.org/10.1038/srep16117.
[63] Wang J, Deng X, Zhang F, Chen D, Ding W. ZnO nanoparticle-induced oxidative stress triggers apoptosis by activating JNK signaling pathway in cultured primary astrocytes. Nanoscale Res Lett 2014;9:117. https://doi.org/10.1186/1556-276X-9-117.
[64] Arakha M, Saleem M, Mallick BC, Jha S. The effects of interfacial potential on antimicrobial propensity of ZnO nanoparticle. Sci Rep 2015;5:9578. https://doi.org/10.1038/srep09578.
[65] Boufas W, Dupont N, Berredjem M, Berrezag K, Becheker I, Berredjem H, Aouf N-E. Synthesis and antibacterial activity of sulfonamides. SAR and DFT studies. J Mol Struct 2014; 1074:180–5. https://doi.org/10.1016/j.molstruc.2014.05.066.
[66] Mubarik A, Rasool N, Hashmi MA, Mansha A, Zubair M, Shaik MR, Sharaf MAF, Awwad EM, Abdelgawad A. Computational Study of Structural, Molecular Orbitals, Optical and Thermodynamic Parameters of Thiophene Sulfonamide Derivatives. Crystals 2021;11:211. https://doi.org/10.3390/cryst11020211.
[67] Mahmood Abdelghani G, Basim Al-Zubaidi A, Ben Ahmed A. Synthesis, characterization, and study of the influence of energy of irradiation on physical properties and biologic activity of nickel ferrite nanostructures. J Saudi Chem Soc 2023;27:101623. https://doi.org/10.1016/j.jscs.2023.101623.
[68] Ben Ahmed A, Feki H, Abid Y, Boughzala H, Minot C, Mlayah A. Crystal structure, vibrational spectra and theoretical studies of l-histidinium dihydrogen phosphate-phosphoric acid. J Mol Struct 2009;920:1–7. https://doi.org/10.1016/j.molstruc.2008.09.029.
[69] Ben Ahmed A, Feki H, Abid Y, Minot C. Molecular structure, vibrational spectra and nonlinear optical properties of orthoarsenic acid–tris-(hydroxymethyl)-aminomethane DFT study. Spectrochim Acta Mol Biomol Spectrosc 2010;75: 1315–20. https://doi.org/10.1016/j.saa.2009.12.073.
[70] Ben Ahmed A, Benhaliliba M, Ocak YS, Ayeshamariam A, Benouis CE. Photovoltaic parameters and computational spectroscopic investigation of third order nonlinear optical of CuPc/Si organic diode. Opt Mater 2022;126:112071. https://doi.org/10.1016/j.optmat.2022.112071.
[71] Benhaliliba M, Ben Ahmed A. The phthalocyanine blue-green pigments devices intended for optical filters. Optik 2022;258:168808. https://doi.org/10.1016/j.ijleo.2022.168808.
[72] Nadafan M, Parishani M, Dehghani Z, Anvari JZ, Malekfar R. Third-order nonlinear optical properties of NiFe2O4 nanoparticles by Z-scan technique. Optik 2017;144:672–8. https://doi.org/10.1016/j.ijleo.2017.06.128.